Effect of grain size on void swelling in irradiated materials: A phase-field approach

Kunok Chang*, Gyeong-Geun Lee and Junhyun Kwon
Nuclear Materials Division, Korea Atomic Energy Research Institute(KAERI), 989-111 Daedeok-daero Yuseong-gu, Daejeon, 305-353, Korea
**Corresponding author: kunokchang@kaeri.re.kr*

1. Introduction

The reliability of irradiated structural alloy is significantly limited by irradiation induced defects, such as voids or gas-filled bubbles [1–4]. Since most structural alloys are polycrystalline materials, understanding the interaction between grain structure and irradiation-induced voids is significantly important. The effect of the grain boundary on the swelling behavior has been investigated by experimental methods [5, 6] and computational methods [7, 8]. An experimental evaluation of the grain size effect on the swelling behavior in irradiated austenitic steel were reported by Singh [5]. In the experiment, swelling decreased with the grain size decreasing below 2.5 μm. This result can be explained by the standard rate theory (SRT). On the other hand, the effect of grain size on the swelling behaviors is quite different when the displacement cascades or subcascades are involved. For example, void swelling enhanced with a grain size decrease in neutron-irradiated polygonized aluminum [9]. Also, the progress of swelling is retarded as the average grain diameter increases in a pure copper case [6]. Within the framework of the production bias model (PBM), their experimental results were quantitatively explained [6]. The phase-field method has already been used to investigate the void/bubble behavior in the irradiated materials [8, 11, 12]. In particular, Millett et al. already incorporated the interaction between the point defect and the grain boundary in their study [8]. Therefore, they described the void denuded zones and void peaked zones adjacent to the grain boundaries [8], which are already observed in the experimental investigations [13–15]. We performed the phase-field simulation in order to verify the role of the grain diameter on the void swelling in the cascade damage condition. In addition, our results will be compared with the experimental observations or the theoretical works, such as PBM.

2. Simulation methods

2.1 Phase-field model for grain structure generation

We adopted the multi-order parameter phase-field grain growth model of ref. [10] to generate the grain structure. According to ref. [10], a single-phase material is represented by a set of non-conserved order parameters η, which are a continuous function of time and space

$$\eta_1(\mathbf{r},t),\ \eta_2(\mathbf{r},t),\ldots,\ \eta_Q(\mathbf{r},t) \quad (1)$$

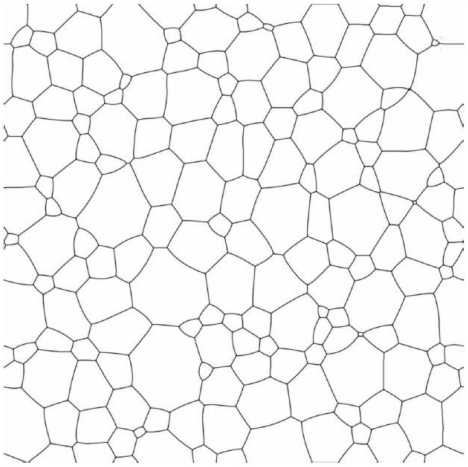

FIG. 1. Grain structure at 120000 Δt. The simulation cell size is 1024 × 1024. 163 grains are present inside the cell and the average grain diameter is 162.9

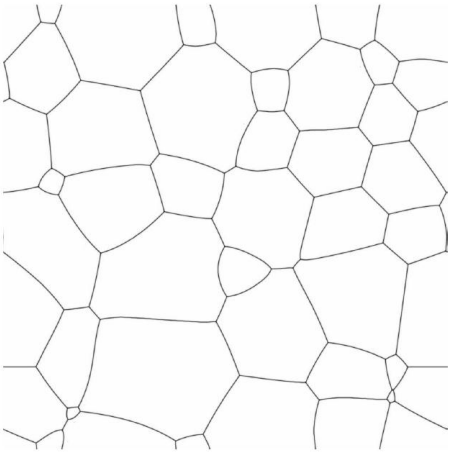

FIG. 2. Grain structure at 600000 Δt. The simulation cell size is 1024 × 1024. 37 grains are present inside the cell and the average grain diameter is 345.2

Each grain is represented by a unique non-conserved order parameter. The temporal and spatial evolutions of the order parameters are described by the time-dependent Ginzburg-Landau equation where the kinetic constant L is related to the grain boundary mobility and the free energy F is a function where the kinetic constant L is related to the grain boundary mobility and the free energy F is a function of the order parameter values and their gradients:

$$F_g = \int_V \left[\sum_i^Q \left(\frac{\eta_i^4}{4} - \frac{\eta_i^2}{2} \right) + \sum_i^Q \sum_{i \neq j}^Q \gamma \eta_i^2 \eta_j^2 + \frac{\kappa}{2} \sum_i^Q (\nabla \eta_i)^2 \right] dV \quad (3)$$

The phenomenological constants κ = 2.0 and γ= 1.0. We implemented the forward Euler scheme to discretize the time and space domain and dt and dx were set to 0.1 and 2.0, respectively [10]. The morphologies from the phase-field grain growth modeling are plotted in Figures 1 and 2. The white and grey regions represent inside grains and grain boundaries. As the growth progresses, the average grain diameter increases (162.9 in Fig. 1 and 345.2 in Fig. 2) and the number of grains decreases from 163 to 37. The microstructures Figures 1 and 2 were visualized by mapping a summation of the square of order-parameter values to a gray scale.

2.2 Phase-field model for void evolution

We introduced the interstitial concentration field ($\mathbf{c}_i(\mathbf{r}, t)$) and the vacancy concentration field ($\mathbf{c}_v(\mathbf{r}, t)$) to simulate the behavior of the point defects. We solved two set of time-dependent partial differential equations

$$\frac{\partial c_i(\mathbf{r},t)}{\partial t} = \nabla M_i \nabla \left(\frac{\delta F}{\delta c_i(\mathbf{r},t)} \right) \quad (4)$$

$$\frac{\partial c_v(\mathbf{r},t)}{\partial t} = \nabla M_v \nabla \left(\frac{\delta F}{\delta c_v(\mathbf{r},t)} \right) \quad (5)$$

$$F = \int_V \left[f(c_i, c_v) + \frac{\kappa_i}{2} (\nabla c_i)^2 + \frac{\kappa_v}{2} (\nabla c_v)^2 \right] dV \quad (6)$$

$$f(c_i, c_v) = \alpha c_i^2 (c_i - 1.0)^2 + \beta c_v^2 (c_v - 1.0)^2 \quad (7)$$

in Eq. 4 and Eq. 5 which were already used in reference [8]. F is the double-well potential with respect to $\mathbf{c}_i$ and $\mathbf{c}_v$ and the minima are located at $\mathbf{c}_i$, $\mathbf{c}_v$ = 0, 1. The phenomenological constants α = β =0.05 and $\mathbf{c}_i$ = $\mathbf{c}_v$ = 0.1. Based on the assumption that the mobility of interstitial is 4 times larger than that of vacancy, we therefore set M_i = 4.0 and M_v = 1.0. We implemented a semi-implicit spectral method to solve Eqs. 4 and 5 as follows: [16]

$$(1+\Delta t \kappa_i k^4) \hat{c_i}^{n+1}(\mathbf{k}) = \hat{c_i}^{n}(\mathbf{k}) - \Delta t k^2 [2\alpha c_i (c_i - 1)(2c_i - 1)]_k \quad (8)$$

$$(1+\Delta t \kappa_v k^4) \hat{c_v}^{n+1}(\mathbf{k}) = \hat{c_v}^{n}(\mathbf{k}) - \Delta t k^2 [2\beta c_v (c_v - 1)(2c_v - 1)]_k \quad (9)$$

where **k** = (k1, k2) is a vector in the Fourier space. After we solved the Eq. 8 and Eq. 9, we incorporated the terms for the point defect production by the radiation damage, vacancy-interstitial recombination and defect sink at the grain boundary.

$$c_i(\mathbf{r}, t+\Delta t) = c_i(\mathbf{r},t) + (P_i(\mathbf{r},t) - R_{iv}(\mathbf{r},t) - S_i^{GB}(\mathbf{r},t))\Delta t \quad (10)$$

$$c_v(\mathbf{r}, t+\Delta t) = c_v(\mathbf{r},t) + (P_v(\mathbf{r},t) - R_{iv}(\mathbf{r},t) - S_v^{GB}(\mathbf{r},t))\Delta t \quad (11)$$

where $P_i(\mathbf{r}, t)$ and $P_v(\mathbf{r}, t)$ are the interstitial and vacancy production via irradiation, respectively and $R_{iv}(\mathbf{r},t)$ is the point defect annihilation through the recombination. $S_{GB}^{i}(\mathbf{r}, t)$ and $S_{GB}^{v}(\mathbf{r}, t)$ are the terms described the interaction of the grain structure with the interstitial and vacancy, respectively. We chose R_1, R_2 between 0 and 1 randomly to described the defect production during the displacement cascade and subcascade. $P_i(\mathbf{r}, t)$ and $P_v(\mathbf{r}, t)$ are defined as follows: $P_i(\mathbf{r}, t) = B \times P_v(\mathbf{r}, t) = B \times R_2 \times 10^{-3}$ when $c_i(\mathbf{r}, t) <= 0.8$ and $c_v(\mathbf{r}, t) <= 0.8$ and the random number R_1 is less than P_{casc} = 0.6. We set the value B to 1.0 (no production bias). Otherwise, $P_i(\mathbf{r}, t) = P_v(\mathbf{r}, t) = 0$. $R_{iv}(\mathbf{r}, t)$ is defined as $R_r \times c_i(\mathbf{r}, t) \times c_v(\mathbf{r}, t)$. R = 0.01.

$$S_i^{GB}(\mathbf{r},t) = S_i^0 (1 - \phi(\mathbf{r},t))(c_i(\mathbf{r},t) - c_i^{eq}) \quad (12)$$

$$S_v^{GB}(\mathbf{r},t) = S_v^0 (1 - \phi(\mathbf{r},t))(c_v(\mathbf{r},t) - c_v^{eq}) \quad (13)$$

where $\phi(\mathbf{r},t) = \Sigma \eta(\mathbf{r},t)^2$ and $\eta(\mathbf{r},t)$ indicates the order parameter in Eq. 2 [8]. In the phase-field grain growth model described above, _(r, t) <= 1.0 [10]. Therefore, $S^{GB}{}_i(\mathbf{r}, t)$ and $S^{GB}{}_v(\mathbf{r}, t)$ are positive or zero in the simulations. $S^0{}_v$ = 0.01 and $c^{eq}{}_i = c^{eq}{}_v = 6.9 \times 10^{-4}$ in our simulations and we varied the $S^0{}_i$ value to examine a role of the efficiency of the interstitial sink at the grain boundary in the swelling process. We applied the periodic boundary condition along the x- and y - directions in all simulations in our study.

3. Results

3.1 Two grains case

The void swelling simulation in the presence of the grain boundary was performed. As shown in Fig. 3, we clearly observed the void denuded zone adjacent to the grain boundary and void peaked zone parallel to the grain boundary. The distance from the grain boundary of the void peaked zone is larger than that of the void denuded zone. This observation is consistent to the previous studies [8, 13–15]. We adopted the parameters S_{GB}^{i} = 0.04 and P_{casc} = 0.2 and the other parameters are all the same with the values written above.

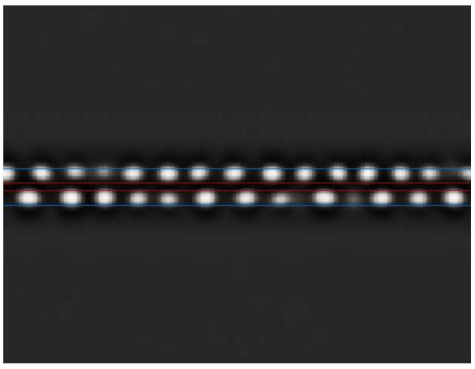

FIG. 3. Distribution of the vacancy concentration at 30000 Δt in the presence of two straight grain boundaries parallel to the x-axis. The void denuded zones (between red lines) and void peaked zones (between blue line and red line) are clearly observed in the figure.

3.2 Many grains case

We performed the phase-field simulations of the swelling process in a polycrystalline material. The progress of swelling in Fig. 4 and Fig. 5 is defined as the ratio of the number of voxels of voids to the total number of voxels. We investigated the distribution of voids by changing the grain structure obtained from another simulation (grain growth modeling in section 2), which are shown in Figures 6 through 9. According to Fig. 4 and Fig. 5, the progress of the swelling was clearly suppressed when the average grain diameter increased. The voids were intensively nucleated and grown at the triple junctions. As the number of grain decreases (average grain diameter increases), the number of triple junctions decreases. Hence, it is more effective to have a large grain diameter to retard the swelling progress in our simulations. In Figures 6 and 7, it is relatively not clear that the triple junctions act as the site for the voids nucleate and grow. The average grain diameter is small in the figures, therefore it is hard to classify whether voids are located at the grain boundaries or the triple junctions. On the other hand, it is much clearer that the triple junctions act as the nucleation and growth sites for the voids in Figures 8 and 9. This conclusion is consistent with the previous experimental observation by Singh et al. [6], which agrees with the prediction within the PBM framework. Since the triple junctions are critical sites for the void nucleation and growth, we observed the triple junction voids in Figures 6 to 9. The triple junction voids have been frequently detected in the experimental observations and it was reported that the triple junction voids significantly induce the fracture process [17–19]. We also estimated the number of voids and average void diameters in our simulations. In general, the number of voids increases as the average grain diameter decreases as shown in Figures 12 and 13. However, there is some exception locally in <D>= 250.75 and <D>= 299.91 in Fig. 13. We examined other set of simulations (with different grain structure and random seed), and this exception was not repeated. Since the number of the observable voids are quite limited in the real experiments and our simulations, the data scattering can affect the final conclusion. In order to reduce the possibility of the misjudgement, we performed two more sets of simulations to confirm the findings. Also, we found that the average void diameter is independent of the average grain diameter, which are shown in Figures 10 and 11. Moreover, we found that both parameter S^0_i and the average grain size significantly affects the degree of swelling. As the average grain diameter increases from 162.92 to 345.21, the degree of swelling increases by a factor of approximately 4 and 8 at 200000_t in Fig. 4 and Fig. 5, respectively. Also, the grain boundary sink efficiency (S^0_i) also critically affects the progress of swelling in our simulations. When S^0_i becomes 0.04, the progress of swelling is approximately 2 times faster than the case of S^0_i = 0.035 (S^0_v=0.01 always). Since $\phi(\mathbf{r}, t)$ values are approximately 0.6 at the triple junctions, 0.7-0.8 at the grain boundaries and approximately 1.0 inside the grain, $S_{GB}{}^i$ (r, t) term should be large at the triple junctions. Therefore, as the interstitial defects disappear, the recombination term $R_{iv}(\mathbf{r}, t)$ decreases. Owing to a decrease of the recombination effect, the vacancy concentration increases at the triple junction in our simulations. If the vacancy sink effect is more dominant than the interstitial-vacancy recombination, the dependency of the swelling progress on the grain size can be changed.

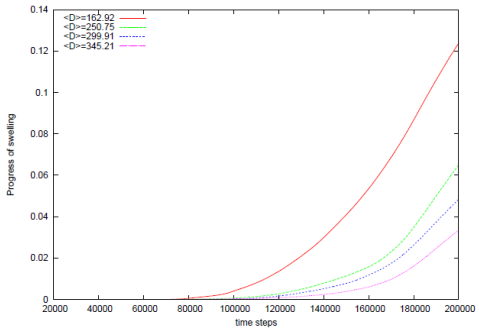

FIG. 4. The progress of swelling as a function of simulation time steps with respect to the average grain diameter. $S_i^0 = 0.04$ in this case.

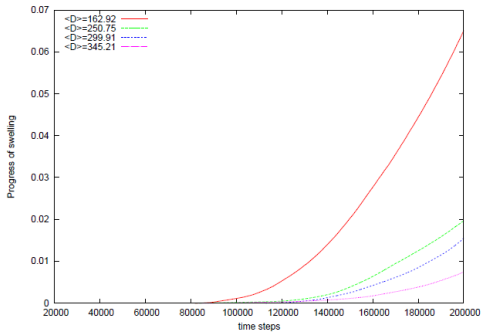

FIG. 5. The progress of swelling as a function of simulation time steps with respect to the average grain diameter. $S_i^0 = 0.035$ in this case.

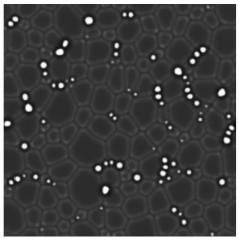

FIG. 6. Two-dimensional distribution of voids at 120000 Δt with the grain structure in Fig. 1. The progress of swelling is 1.36% and the average diameter of the void is 15.49 grid points and 65 voids are present in the simulation cell.

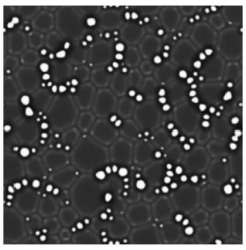

FIG. 7. Two-dimensional distribution of voids at 150000 Δt with the grain structure in Fig. 1. The progress of swelling is 4.19% and the average diameter of the void is 17.26 grid points and 154 voids are present in the simulation cell.

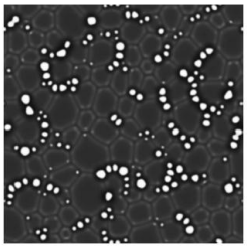

FIG. 7. Two-dimensional distribution of voids at 150000 Δt with the grain structure in Fig. 1. The progress of swelling is 4.19% and the average diameter of the void is 17.26 grid points and 154 voids are present in the simulation cell.

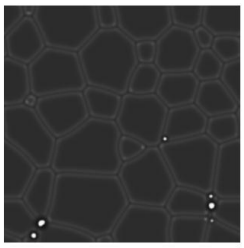

FIG. 8. Two-dimensional distribution of voids at 120000 Δt with the grain structure in Fig. 2. The progress of swelling is 0.09% and the average diameter of the void is 14.00 grid points and 5 voids are present in the simulation cell.

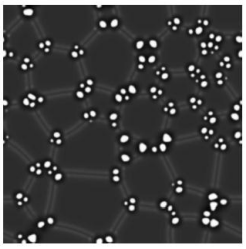

FIG. 9. Two-dimensional distribution of voids at 200000 Δt with the grain structure in Fig. 2. The progress of swelling is 3.35% and the average diameter of the void is 17.64 grid points and 129 voids are present in the simulation cell.

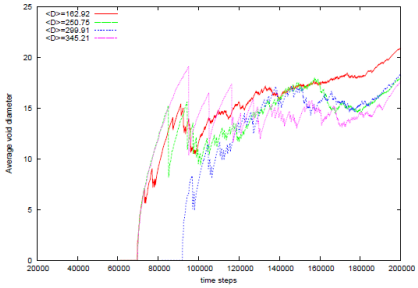

FIG. 10. Average void diameter to the simulation time steps. We used $S_i^0 = 0.04$.

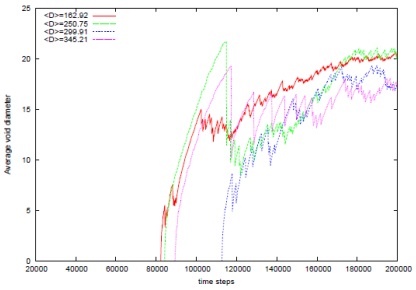

FIG. 11. Average void diameter to the simulation time steps. We used $S_i^0 = 0.035$.

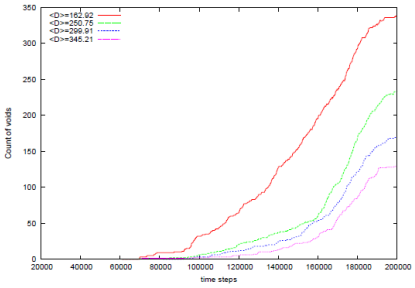

FIG. 12. Number of voids as a function of simulation time steps with respect to the average grain diameter. We used $S_i^0 = 0.04$.

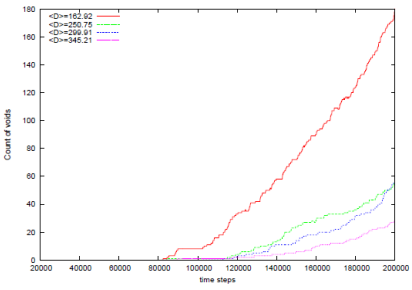

FIG. 13. Number of voids as a function of simulation time steps with respect to the average grain diameter. We used $S_i^0 = 0.035$.

3. Conclusions

Two-dimensional phase-field simulations were performed to investigate the void swelling process in the

irradiated materials. We clearly observed the void denuded and void peaked zones, which were already observed in formal experimental and computational approaches. We also found that the progress of swelling was retarded as the average grain diameter increased. The triple junctions, which are believed to be a critical factor t affecting the fracture, are the main cites for the void nucleation and growth in our simulations.

REFERENCES

[1] Little EA, Stow DA. Jour Nuc Mater 1979;87:25
[2] Singh BN, Foreman AJE. Phil Mag A 1992;66:975
[3] Zinkle SJ, Maziasz PJ, Stoller RE. Jour Nuc Mater 1993;206:266
[4] Dubinko VI. Jour Nuc Mater 1993;206:1
[5] Singh BN. Phil Mag 1974;29:25
[6] Singh BN, Eldrup M, Zinkle SJ, Golubov SI. Phil Mag A 2002;82:1137
[7] Yang Y, Huang H, Zinkle SJ. Jour Nuc Mater 2010;405:261
[8] Millett PC, El-Azab A, Rokkam S, Tonks M, Wolf D. Comp Mater Sci 2011;50:949
[9] Horsewell A, Singh BN. ASTM Spec Techni Publi 1987;955:220
[10] Chen LQ, Yang W. Phys Rev B 1994;50:15752
[11] Hu S, Henager Jr. CH, Heinisch HL, Stan M, Baskes MI, Valone SM. Jour Nuc Mater 2009;392:292
[12] Semenov AA, Woo CH. Acta Mater 2012;60:6112
[13] Kulcinski GL, Mastel B, Kissinger HE. Acta Metall 1971;19:27
[14] Konobeev YV, Tsherbak VI, Bykov VN, Subbotin AV. Phys Stat Sol A 1975;29:121
[15] Konobeev YV, Tsherbak VI, Bykov VN, Subbotin AV. Phys Stat Sol A 1977;40:89
[16] Zhu JZ, Chen LQ, Shen J, Tikare V. Phys Rev E 1999;60:3564
[17] Park H, Hwang SJ, Joo YC. Acta Mater 2004;52:2435
[18] Ovidko IA. Jour of Mater Sci 2007;42:1694
[19] Shan Z, Knapp JA, Follstaedt DM, Stach EA, Wiezorek JMK, Mao1 SX. Phys Rev Lett 2008;100:105502